



Dynamics and scaling in quasi-two-dimensional turbulent convection

C. Bizon^{a,*}, A.A. Predtechensky^a, J. Werne^b, K. Julien^c,
W.D. McCormick^a, J.B. Swift^a, H.L. Swinney^a

^a *Center for Nonlinear Dynamics and Department of Physics, University of Texas, Austin, TX 78712, USA*

^b *Joint Institute for Laboratory Astrophysics and Laboratory for Atmospheric and Space Physics, University of Colorado, Boulder, CO 80309, USA*

^c *Advanced Study Program, National Center for Atmospheric Research, Boulder, CO 80307, USA*

Abstract

High Rayleigh number ($4 \times 10^4 - 3 \times 10^7$) quasi-two-dimensional convection is studied experimentally, numerically, and theoretically. The fluid is contained in an isothermal Hele-Shaw cell, which enforces the two dimensionality, and the convection is driven by an externally imposed vertical concentration gradient. The full two dimensional concentration field is imaged experimentally and is sampled at regular intervals spanning between five and fifty convective times (the time it takes a plume to cross the cell). The most prominent and dynamically significant features of the flow are solutal plumes which form within the concentration boundary layer. Tip splitting of plumes leading to smaller length scales and merging of plumes leading to larger length scales are observed. A model of Hele-Shaw convection, which includes a friction term due to the boundaries parallel to the velocity field, is simulated. The evolution of the pattern and dynamics of the concentration field, as well as time averaged spatial spectra, are obtained from the experiment and simulation. Results for exponents which describe how the Nusselt number and Reynolds number scale with Rayleigh number are obtained theoretically and compared with the values from simulation.

1. Introduction

A fluid undergoing turbulent convection is a canonical example of a system which is far from equilibrium, which contains many spatial scales, and has a wide variety of useful applications. As such, it has generated a large amount of research [1], most of which has justifiably focused on the case of convection in three dimensions. However, compelling reasons exist to conduct studies limited to two dimensions. Experimentally,

* Corresponding author. E-mail: bizon@chaos.ph.utexas.edu.

the entire scalar field may be imaged. Also, two dimensional numerical simulations allow the computation of dynamics at much higher Rayleigh numbers [2]. No physical flows are strictly two-dimensional, although important physical systems such as the stratosphere may be considered quasi-two-dimensional. In such systems, velocity and scalar fields are treated two-dimensionally, but effects of the third dimension are incorporated into the evolution equations for these fields [3].

Guided by such considerations, we study turbulent convection in a quasi-two-dimensional system, namely, in a Hele-Shaw cell. Experimentally, the density gradient which drives the convection is produced by an externally imposed concentration gradient [4], in contrast with previous studies with thermal driving [5,6]. Further, the values of the diffusion constant D and kinematic viscosity ν provide a Schmidt number σ (the analog of the Prandtl number in thermal convection) of order 10^3 .

In Section 2 we briefly describe the experimental arrangement. In Section 3 we give the model, highlighting the differences between the more commonly known Rayleigh-Bénard convection and our Hele-Shaw convection, and we discuss the simulation methods. In Section 4 we present results and discussion.

2. Experimental arrangement

The convection cell is a rectangular parallelepiped, with dimensions $L = 240 \text{ mm} \times L = 240 \text{ mm} \times \delta = 1 \text{ mm}$. One of the sides of length L is parallel to gravity. A vertical density gradient is imposed in this isothermal cell via a concentration gradient; the top and bottom bounding surfaces are thin membranes, connecting the cell to continuously refreshed reservoirs containing solutions of iodine in ethyl alcohol. The use of solute as the convective scalar enforces perfect no-flux boundary conditions on the $L \times L$ side walls – a condition which was not met in studies of thermally driven Hele-Shaw convection [5,6]. At the highest Rayleigh number achieved, $Ra^* = 3.3 \times 10^7$, the iodine concentrations at the top and bottom surfaces were 5.0% and 0.5%, respectively. At the high Rayleigh numbers studied, the rate of diffusion of solute in the membranes is comparable to that in the fluid, in contrast to thermally driven flow, where the horizontal boundaries can be constructed with high conductivity materials. In order to provide well defined concentrations at the boundary, therefore, fluid was slowly pumped in through the membranes and out through similar gaskets at the narrow vertical bounding walls. In the experiments the vertical velocities at the boundaries due to the pumping were about 15% of the rms vertical velocity in the core. Even this relatively weak pumping changes the nature of the thin concentration boundary layer. The ratio of convective to conductive flux through the boundary layer is given by the boundary Peclet number, $w_{\text{pump}}\lambda/D$, where w_{pump} is the velocity of the boundary pumping, and λ is the depth of this layer. In our experiments, the Peclet number is of the order 10^3 , indicating a highly convective boundary layer.

The concentration field was imaged by taking advantage of the blue light absorption of iodine; see Fig. 1. Images were taken by a video camera and recorded on a computer

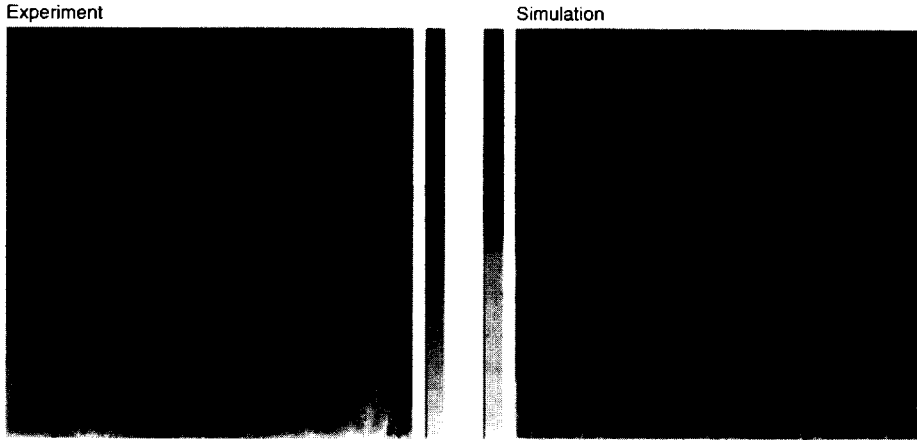


Fig. 1. Full images of the turbulent, convective, two-dimensional concentration field. Plumes form in the boundary layer, and merge to form vertical channels. The cell is $L \times L$, and has thickness δ perpendicular to the page. Both images have $Ra^* = 1.0 \times 10^7$. The experimental cell has $\delta/L = 1/240$, while the simulation, which has no-slip horizontal boundaries, is conducted at $\delta/L = 1/20$.

disk at regular intervals ranging from 30 s at the lowest Rayleigh number (3.0×10^6) to 2 s for the highest. Several hundred images were recorded for each run. These data sets cover between five and fifty convective times, the time it takes for a solutal plume to cross the cell.

3. Model

The x and z coordinate axes are chosen parallel to the sides of length L and the y axis to that of length δ . Because δ is much less than L , the flow parallel to the side walls may be turbulent, while the crosswise Reynolds number, $u\delta/\nu$, is no larger than of order ten. This allows the assumption of a parabolic velocity profile in the y direction. Similarly, the lowest order assumption for the concentration consistent with no-flux boundary conditions is that the concentration is independent of y . Inserting these profiles into the Navier–Stokes equations in the Boussinesq approximation, averaging over y , and nondimensionalizing with respect to the length L , the time L^2/D , and the concentration difference Δ leads to the following two-dimensional model [7],

$$\partial_t \mathbf{u} + \frac{4}{5} \omega_y \hat{y} \times \mathbf{u} = \sigma \left[\nabla_{\perp}^2 - 12 \left(\frac{L}{\delta} \right)^2 \right] \mathbf{u} - \nabla P - \frac{3}{2} \sigma Ra c \hat{z}, \quad (1)$$

$$\partial_t c + \frac{2}{3} \mathbf{u} \cdot \nabla c = \nabla_{\perp}^2 c, \quad (2)$$

$$\nabla \cdot \mathbf{u} = 0. \quad (3)$$

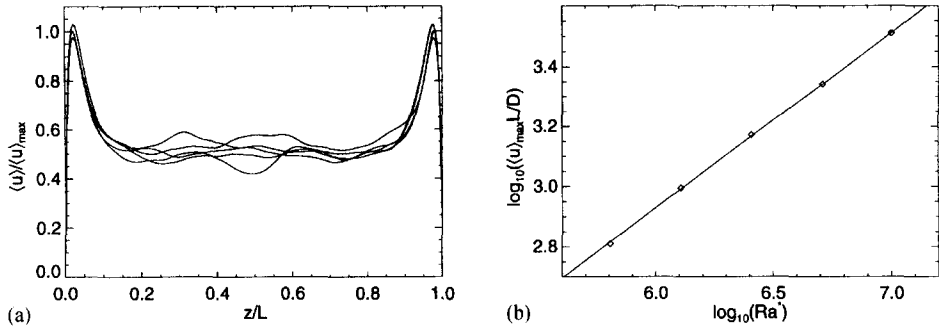


Fig. 2. (a) These graphs of RMS horizontal velocity as a function of height, obtained in simulations with $\delta/L = 1/20$, reveal that the velocity boundary layers have width $\delta/2$, independent of Ra^* – the curves are for Ra^* 's ranging from 6.4×10^5 to 1.0×10^7 and each has been divided by $\langle u \rangle_{\max}$, the average of its two maxima (one near each boundary), to make the profiles overlap. In the core the RMS horizontal velocity is independent of z , but as plumes approach a boundary, they slow vertically and spread out horizontally, resulting in a peak in the horizontal velocities at a distance about $\delta/2$ from the boundary. Closer to the boundary, the gradient diffusion term dominates the linear Hele-Shaw drag term in the momentum equation. Slight asymmetry (less than 5%) is observed for some of these profiles, probably due to imperfect statistics. (b) This plot displays the scaling of $\langle u \rangle_{\max}$ with Ra^* . The line is given by a weighted linear least squares fit as $\log_{10}(\langle u \rangle_{\max} L/D) = (-0.56 \pm 0.04) + (0.58 \pm 0.01) \log_{10}(Ra^*)$.

Here \mathbf{u} , P , and c are the two-dimensional velocity, pressure, and solute concentration fields of the fluid. The parameters ν and D are the kinematic viscosity and solutal diffusivity, respectively. Gravity \mathbf{g} is directed downward, in the negative z direction. The subscript \perp refers to the x – z plane, and ω_y is the y component of $\nabla_{\perp} \times \mathbf{u}$, the vorticity. Also, $\sigma = \nu/D$ and $Ra = g\beta\Delta L^3/(\nu D)$ are the Schmidt and solutal Rayleigh numbers. In addition, the pressure has absorbed contributions $\propto c_o z$ from the mean solute concentration and $\propto u^2/2$ from the nonlinear term, as well as numerical and dimensional factors.

Apart from numerical factors, the difference between these equations and the two dimensional Boussinesq Navier–Stokes equations is the extra dissipation term in Eq. (1) proportional to the velocity. Because the scale of flow structures is larger than δ , the $\nabla_{\perp}^2 \mathbf{u}$ term is outweighed by this linear Hele-Shaw drag term. Near no-slip boundaries, the gradient term must assert itself. This implies velocity boundary layers of order δ for no-slip boundaries. We observe such boundary layers in simulations; see Fig. 2 and below. As δ/L decreases, the velocity boundary layer becomes more shallow, and in the strict Hele-Shaw limit, $\delta/L \rightarrow 0$, the boundary layer is infinitely thin. A linear stability analysis of Eqs. (1)–(3) reveals that in this limit, the critical Rayleigh number and critical wave number are the same for no-slip and stress-free boundaries [7,8]. Also, corrections to the strict limit appear at a higher order in δ/L for the stress-free as compared to the no-slip case. Since the competition between the gradient and linear friction terms in Eq. (1) does not explicitly involve the nonlinear terms, stress-free boundary conditions should be applicable to high Rayleigh numbers as well as near onset. Linear stability analysis also reveals that the control parameter for Hele-Shaw

convection is not Ra , but $Ra^* = Ra(\delta/L)^2$. All Rayleigh numbers given herein are Ra^* 's.

We perform numerical simulations of Eqs. (1)–(3); see Fig. 1. Spectral decompositions of \mathbf{u} , P and c are evolved through the hybrid-implicit/explicit 3rd-order Runge–Kutta scheme of Spalart et al. [9]; we treat nonlinear terms explicitly and the remaining linear terms implicitly [7]. Calculations have been performed with the experimental values of $\sigma = 1000$ and $\delta/L = 1/240$. At such a small cell width, the no-slip velocity boundary layer becomes extremely difficult to resolve. Guided by the results of linear stability, our runs at this width, as well as runs with $\delta/L = 1/20$ are performed with stress-free horizontal boundaries. At the larger value of δ , no-slip velocity boundary layers are correspondingly larger and we also perform simulations with no-slip horizontal boundaries. All simulations have constant concentrations at top and bottom boundaries, and the vertical boundaries are stress-free and no-flux.

4. Results

When the time and horizontally averaged concentration is examined as a function of height, both experiment and simulation exhibit thin solutal boundary layers near the top and bottom surfaces and a core region in which the concentration is essentially independent of z . The most prominent features of instantaneous images of the concentration field are plumes which arise from the solutal boundary layers, as displayed in Fig. 1. Plume merging, shown in Fig. 3, and tip splitting of plumes, seen in Fig. 4, are observed. These phenomena are the configuration space realizations of concentration cascades in Fourier space. Time averaged spatial power spectra exhibit anisotropy at large length scales with increasing isotropy at smaller length scales in accord with a cascade picture of turbulence.

A question of much interest in the study of high Rayleigh number convection is that of the scalings of the Nusselt number (the dimensionless heat flux, Nu) and Peclet number (the dimensionless rms velocity $wL/D = \sigma wL/\nu = \sigma Re$) with Rayleigh number. We have constructed a theory for the scalings measured from simulation data. Because of the insensitivity of Hele-Shaw convection to the form of the velocity boundary conditions, we are able to find a scaling law related to plumes in the turbulent core, which holds for both no-slip and stress-free runs. We note that it is the concentration



Fig. 3. Solutal plumes rise just above the concentration boundary layer in this simulation for $Ra^* = 3.2 \times 10^5$ ($\delta/L = 1/240$; stress-free horizontal boundaries). The plumes form through a Rayleigh–Taylor instability at the boundary layer and carry solute away from the boundary. Plumes moving in the opposite direction create a horizontal velocity (see Fig. 2) that advects plumes into one another. They merge and form channels that cross the cell vertically (see Fig. 1). The image displays the lowest one tenth of the cell.

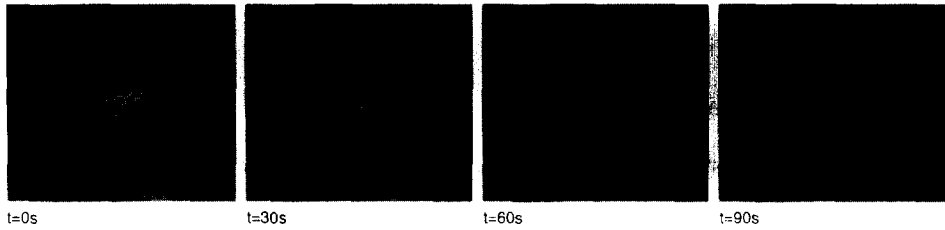


Fig. 4. Experimental sequence of splitting plumes showing the collision of a rising (light) plume with a falling (dark) plume ($Ra^* = 2.0 \times 10^7$). The interface between the plumes has a large density gradient and develops a Rayleigh–Taylor instability. This splitting is common in the experiment where the boundary pumping causes plumes to have enhanced concentration. The snapshots are a section of the turbulent core and have dimensions $0.32 L \times 0.28 L$.

and velocity of the plumes which determine the rms concentration and velocity. Plumes are responsible for carrying solute away from the concentration boundary layers. As they rise, their buoyancy is balanced by the Hele-Shaw drag, and they reach a terminal velocity. These arguments combine to give

$$Pe^2 \sim Ra^* Nu. \quad (4)$$

We achieve good agreement between this equation and data from both no-slip and stress-free boundary conditions, which cover a combined range in Ra^* from 4.0×10^4 to 1.0×10^7 [7].

Another scaling law derives from considering flow near the solutal boundary layers. Since, in some cases, the velocity boundary layers are larger than the solutal layers, this law will be dependent on the velocity boundary conditions. For stress-free boundary conditions, plumes merge to form long lived vertical solute conduits. The image from simulation in Fig. 1 displays channels for no-slip boundary conditions, which are similar, but more transitory. We model the velocity field near the boundary layers and follow arguments similar to those of Ref. [10]. These considerations give a second scaling law (for stress-free boundary conditions) as

$$Nu \sim (n Pe)^{1/2}, \quad (5)$$

where n is the average number of plumes. We have extracted n from the simulations based on the fact that near the base of a plume the horizontal velocity has a negative horizontal gradient. With this input, we may compare Eq. (5) to the scaling measured from the simulation. The agreement is satisfactory for all stress-free runs, for which Ra^* varies between 4.0×10^4 and 2.56×10^6 [7].

For no-slip boundaries, horizontal motion of plumes is hindered, and both channels and the boundary layer acquire a time dependence. Hence, a long region of sheared flow like that described in Ref. [10] never develops and such arguments are inappropriate. In our no-slip runs, the thermal boundary layer is entirely contained within the deeper velocity boundary layer. It will be governed, then, by the gradient, rather than the linear, dissipation term, and the appropriate control parameter for the boundary layer

is Ra rather than Ra^* . Priestley's argument [11] regarding communication between boundary layers then implies that

$$Nu \sim Ra^{*1/3} (L/\delta)^{2/3}. \quad (6)$$

While there is small systematic deviation from this equation, the agreement is surprisingly good over the full no-slip Ra^* range of 3.2×10^5 – 1.0×10^7 [7].

The effects of the linear drag term are ubiquitous. It stabilizes flow structures with a small horizontal scale, allowing plumes and channels to form, rather than the turbulent roll observed in simulations of 2D Rayleigh–Bénard convection [2]. The dissipation in the cell is strongest in the core, again in contrast to Rayleigh–Bénard convection, where sheared boundary layers determine dissipative scaling behavior [10]. By changing the nature of the drag, an equilibrium between buoyancy and drag is achieved which has a different form than that for Rayleigh–Bénard convection, leading to different exponents in the scaling laws. This term also causes the insensitivity to velocity boundary conditions, which is complete in the perfect Hele-Shaw limit, and which we suggest is a widespread feature of quasi-two-dimensional flows.

Acknowledgements

This research was supported by the US Department of Energy Office of Basic Energy Sciences and the Texas Advanced Research Program. NCAR is sponsored by the National Science Foundation. J.W. is supported by the NSF High Performance Computing and Communication grant ECS9217394.

References

- [1] E. Siggia, *Ann. Rev. Fluid Mech.* 26 (1994) 137.
- [2] E.E. DeLuca, J. Werne, R. Rosner and F. Cattaneo, *Phys. Rev. Lett.* 64 (1990) 2370; J. Werne, E.E. DeLuca, R. Rosner and F. Cattaneo, *Phys. Rev. Lett.* 67 (1991) 3519; J. Werne, *Phys. Rev. E* 48 (1993) 1020.
- [3] S.D. Danilov, F.V. Dolzhanskii and V.A. Krymov, *Chaos* 4 (1994) 299.
- [4] A.A. Predtechensky, W.D. McCormick, J.B. Swift, A.G. Rossberg and H.L. Swinney, *Phys. Fluids* 6 (1994) 3923.
- [5] B.K. Hartline and C.R.B. Lister, *J. Fluid Mech.* 79 (1977) 379.
- [6] J.N. Koster and U. Muller, *J. Fluid Mech.* 125 (1982) 429; *Phys. Rev. Lett.* 47 (1981) 1599; *J. Fluid Mech.* 139 (1984) 363.
- [7] C. Bizon, J. Werne, A.A. Predtechensky, K. Julien, W.D. McCormick, J.B. Swift and H.L. Swinney, *Chaos* 7 (1997) 107.
- [8] K. Julien and J. Werne, to be submitted.
- [9] P.R. Spalart, R.D. Moser and M.M. Rogers, *J. Comput. Phys.* 96 (1991) 297.
- [10] B. Shraiman and E. Siggia, *Phys. Rev. A.* 42 (1990) 3650.
- [11] C.H.B. Priestley, *Australian J. Phys.* 7 (1954) 176.